THE ASTROPHYSICAL JOURNAL, 463:395–403, 1996 June 1

DEVIATIONS FROM HIERARCHICAL CLUSTERING IN REAL AND REDSHIFT SPACE

SEBASTIANO GHIGNA[1] AND SILVIO A. BONOMETTO[1]
Dipartimento di Fisica dell'Università di Milano, via Celoria 16, I-20133 Milano, Italy
LUIGI GUZZO
Osservatorio Astronomico di Brera-Merate, via Bianchi 46, I-22055 Merate (CO), Italy
RICCARDO GIOVANELLI[2] AND MARTHA P. HAYNES[2]
Department of Astronomy, Space Sciences Building, Cornell University, Ithaca, NY 14853-6801
ANATOLY KLYPIN[3]
Astronomy Department, New Mexico State University, Box 30001/Dept. 4500, Las Cruces, NM 88003-0001
AND
JOEL R. PRIMACK
Institute for Particle Physics, University of California, Santa Cruz, Santa Cruz, CA 95064
Received 1994 May 2; accepted 1995 December 13

ABSTRACT

Redshift-space distortions interfere with the estimation of high-order galaxy correlation functions. We find that deviations from hierarchical scaling of the galaxy distribution cannot be evaluated in redshift space. In addition, we show that an empirical technique, previously used to tentatively eliminate redshift-space distortions and able to recover the correct behavior of the two-point function, heavily interferes with higher order function estimates. These conclusions are attained by analyzing both observational data (the Perseus-Pisces redshift survey [PPS]) and the results of 512^3 cell particle-mesh simulations for cold dark matter and cold plus hot dark matter models. Using the neighbor-moment approach, we detect modest but significant deviations from hierarchical scaling in real space for simulated data. These are consistent with expectations for an initially biased galaxy field, once we take into account the displacements from the sites where galaxies formed due to observed nonlinear gravitational evolution. The passage to redshift space has the net effect of filtering out such distortions. Still on simulated data, taken in redshift space, we apply the empirical technique previously used on PPS data, aimed at *reconstructing* the real-space galaxy distribution. This technique is found to magnify the deviations from the hierarchical behavior of real-space data, if such deviations exist, and risks creating them artificially. Finally, the analysis of PPS data reveals a behavior similar to that seen in the simulations, both in redshift space and in *reconstructed* real space.

Subject headings: galaxies: clusters: general — galaxies: distances and redshifts — large-scale structure of universe

1. INTRODUCTION

The large-scale mass distribution in today's universe is well known to be non-Gaussian. A detailed analysis of n-point ($n > 2$) correlation functions aims to discriminate among different kinds of non-Gaussian processes. In turn, an advanced knowledge of the non-Gaussian process that describes today's world is a potential discriminator among different theoretical views on the origin of the present large-scale structure.

In this paper we report the results of an analysis of n-point ($n = 3, 4$) functions based on the neighbor-moment evaluation. We discuss the effect of redshift-space distortions on these statistics, using the Perseus-Pisces redshift survey (PPS) data together with realistic artificial galaxy samples extracted from the N-body simulations of Klypin, Nolthenius, & Primack (1995). Our aim is to compare results in real and redshift space.

While, for simulated data, it is straightforward to work in either real or redshift space, from the observational point of view direct information on true galaxy distances (and thus on their peculiar velocities) is available only for restricted samples, typically limited to ~ 6000 km s^{-1}. Therefore, no direct information is available on the real-space distribution for most of the galaxies in large redshift surveys such as PPS, although a number of efforts are being carried on in that direction (e.g., Giovanelli & Haynes 1996).

Statistical estimators can be affected by the fact of mapping the universe in redshift space. In the case of the two-point function $\xi(r)$, significant distortions arise because of two main reasons: (1) on small scales, $\xi(r)$ is depressed because of the redshift-space elongation of high velocity dispersion regions (rich clusters); (2) at large separations, $\xi(r)$ is amplified because of coherent motions toward overdense regions and away from underdense regions (Kaiser 1987).

These effects can be appreciated by splitting the separations of galaxy pairs into their components θ and π (parallel and perpendicular to the line of sight, respectively) and comparing the two-point functions evaluated with respect to each component (see, e.g., Davis & Peebles 1983; Fisher et al. 1994). A similar decomposition can be performed on the power spectrum $P(k)$ (see, e.g., Cole, Fisher, & Weinberg 1994, 1995). A number of investigations of redshift-space distortions for two-point statistics [$\xi(r)$ or $P(k)$] have also been performed using N-body simulations (see, e.g., Gramann, Cen, & Bahcall 1993).

[1] INFN, Sezione di Milano, Italy.
[2] National Astronomy and Ionosphere Center (NAIC is operated by Cornell University under a cooperative agreement with the National Science Foundation).
[3] Astro Space Center, Lebedev Physical Institute, Moscow, Russia.

Redshift-space distortions on the higher moments of galaxy distribution have recently been addressed by Matsubara & Suto (1994), Suto & Matsubara (1994), and Bonometto et al. (1994, hereafter BBGKP). The former two authors made use of cold dark matter (CDM) simulations only. In the latter paper, the simulations considered here were already partially considered.

A previous analysis of three- and four-point functions, using neighbor moments (Bonometto et al. 1993, hereafter BIGGH), was performed on PPS data, corrected by statistically collapsing each Abell cluster to its most probable spatial size, so eliminating the large "fingers of God" that PPS contains. This operation allowed recovery of the correct shape of $\xi(r)$ at small scales. After such correction, the PPS data showed deviations of three- and four-point functions from a pure hierarchical model (HM) behavior (for the definition of HM see, e.g., Groth & Peebles 1977; Fry & Peebles 1978; Sharp, Bonometto, & Lucchin 1984; see also eqs. [2], [3]).

Our aim here is to explore two points: (1) the influence of using data in redshift space on the detection of deviations from HM behavior and (2) the reliability of the real-space data reconstruction technique used in BIGGH to detect deviations from HM in observational data.

Using simulations, we find that deviations from HM behavior are widely erased by the passage to redshift space. This is to be related to the peculiar velocities of galaxies, v_p, which cause displacements from their formation sites on the order of v_p/H within a time $\sim H^{-1}$ (the Hubble time). Such displacements can be expected to interfere with deviations from HM behavior up to scales $\sim v_p/H$, and their effect is certainly strengthened and even extended to larger scales by the passage to redshift space, which adds an apparent displacement, still $\sim v_p/H$, to the physical one. In this sense the passage to redshift space is a "magnifier" of nonlinear effects, expected to delete deviations from HM behavior.

If we now apply to simulated data in redshift space the technique used to *compress* the "fingers of God" (as in PPS data), we find again deviations from HM behavior. Qualitatively, such deviations are similar to the ones previously erased by the passage to redshift space, but their size is systematically larger.

Using PPS data in redshift space, we also find no indication of significant deviations from HM behavior, quite different from the findings of BIGGH on PPS data after finger-of-God compression. According to the above analysis of simulations, this is to be expected, and it is possible that deviations from HM in PPS are an actual feature of the real-space distribution. However, our results on simulated data show that a safe estimate of the quantitative impact of the simple compression technique considered here is hard to make.

Before giving the plan of the paper, it is worth listing the data sets used to evaluate moments in this work. All are *observational* or *artificial* volume-limited samples (VLSs). From simulations we obtained three artificial VLSs: in *real* space, in *redshift* space, and in the *reconstructed* space. The VLSs obtained from PPS, instead, are obviously only two: in redshift space and in the reconstructed space.

We start from the analysis of PPS data, which is described in § 2. We report the statistical measures that we have performed on the redshift-space VLS and compare them with similar measures for the reconstructed-space VLS obtained by BIGGH. In § 3, we describe the simulations used and the technique we adopt to build artificial galaxy samples from them. Such samples provide us the artificial VLSs in real, redshift, and reconstructed space. Statistical analysis is performed for these three cases. In § 4, we compare the results for observational and simulated data and draw our conclusions.

2. PPS RESULTS

The PPS database was compiled by Giovanelli & Haynes during the last decade (see Giovanelli & Haynes 1991). It consists mainly of highly accurate 21 cm H I line redshifts, partly unpublished, obtained with the NAIC 305 m telescope in Arecibo[4] and with the NRAO[5] 300 foot (91.44 m) telescope formerly in Green Bank, West Virginia (Giovanelli, Haynes, & Chincarini 1986; Haynes et al. 1988; Giovanelli & Haynes 1989). The radio data are complemented with optical observations of early-type galaxies carried out at the 2.4 m telescope of the McGraw-Hill Observatory[6] (Wegner, Haynes, & Giovanelli 1993). In order to exclude regions of sky of high Galactic extinction, we limited the sample to the region bound by $22^h \leq \alpha \leq 3^h10^m$, $0° \leq \delta \leq 42°30'$. We then selected, after correcting Zwicky magnitudes (m_{Zw}) for extinction using the absorption maps of Burstein & Heiles (1978), all galaxies brighter than $m_{Zw} = 15.5$. The resultant sample is 98% complete to this limiting magnitude and includes 3395 galaxies.

In addition to the increased completeness, the sample used here differs from that used in BIGGH in that no correction was applied to the observed velocities, apart from the transformation to put the observer at rest with respect to the cosmic background radiation frame of reference. For the analysis of PPS performed in BIGGH, instead, velocity corrections were made to compensate for the Galactic rotation and the motion of the Galaxy within the Local Group, while a suitable simplified model was used to correct also for Virgocentric flow. They did not apply only to the observer, but also to galaxies at a distance smaller than Virgo or comparable with it. The net effect of all these velocity corrections was close to that of those applied by Yahil, Tammann, & Sandage (1977).

As a further correction, a simple algorithm was applied to all the Abell $R > 1$ clusters in PPS in order to reduce the impact of finger-of-God distortions on global correlations extracted from the data. According to the analysis we present in this paper, this last correction had a number of secondary effects. We shall therefore discuss it in more detail below.

As in BIGGH, our statistical analyses are performed on a volume-limited sample, obtained by requiring that galaxies have $M \leq -19 + 5 \log h$ and distance $d \leq 79\, h^{-1}$ Mpc (h is the Hubble constant in units of 100 km s^{-1} Mpc^{-1}). In this new version, the VLS contains 902 galaxies. This is smaller than the VLS used in BIGGH, in spite of the increased completeness of the current version of PPS. This decrease is due to the fact that, in the cosmic background radiation

[4] The Arecibo Observatory is part of the National Astronomy and Ionosphere Center, operated by Cornell University under a cooperative agreement with the National Science Foundation.

[5] The National Radio Astronomy Observatory is operated by Associated Universities, Inc., under a cooperative agreement with the National Science Foundation.

[6] The McGraw-Hill Observatory is located on Kitt Peak and jointly operated under a cooperative agreement by Dartmouth College, the Massachusetts Institute of Technology, and the University of Michigan.

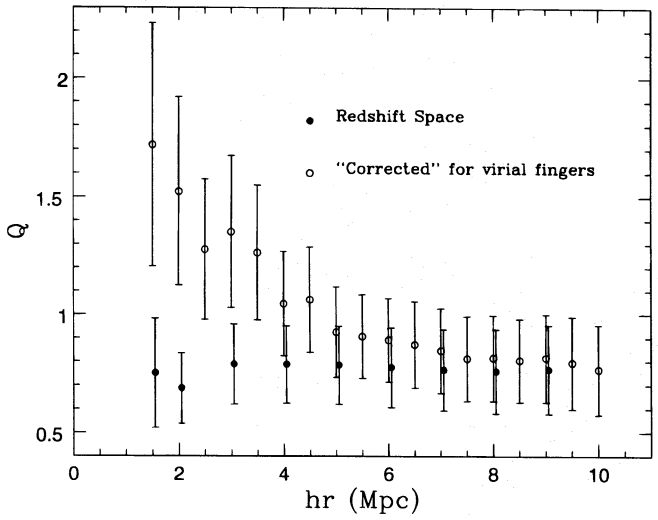

FIG. 1.—Hierarchical coefficient Q of the three-point function for the $M \leq 19$, $d \leq 79\ h^{-1}$ Mpc volume-limited sample of the Perseus-Pisces redshift survey shown as a function of the scale r. Q is evaluated by the neighbor-count technique using spheres of radius r and is expected to be a constant if the hierarchical model holds. Filled circles refer to the distribution of galaxies with distances obtained through redshifts (redshift space). Open circles refer to the sample in which a number of corrections (for virial fingers and Virgo infall) have been applied in a tentative reconstruction of the real-space distribution at small scales. Open circles have been slightly displaced to the right to avoid overlapping of error bars. The latter are estimated by a bootstrap-like method and correspond to 3 σ.

frame of reference, several galaxies ought to be considered to be significantly nearer to the observer. Their apparent luminosity is therefore turned into a smaller intrinsic luminosity, and when comparing such luminosities to the magnitude limit of the VLS, several galaxies fall below such limit.

Let us now discuss in more detail the algorithm that was applied to the Abell $R > 1$ clusters in PPS in the attempt of reducing the impact of finger-of-God distortions on global correlations. In order to appreciate its effects, an analogous procedure will be applied here to simulated data.

In general, a spherical cluster of galaxies appears in redshift space as an elongated "finger" as a result of its high internal velocity dispersion. The velocity distribution is well

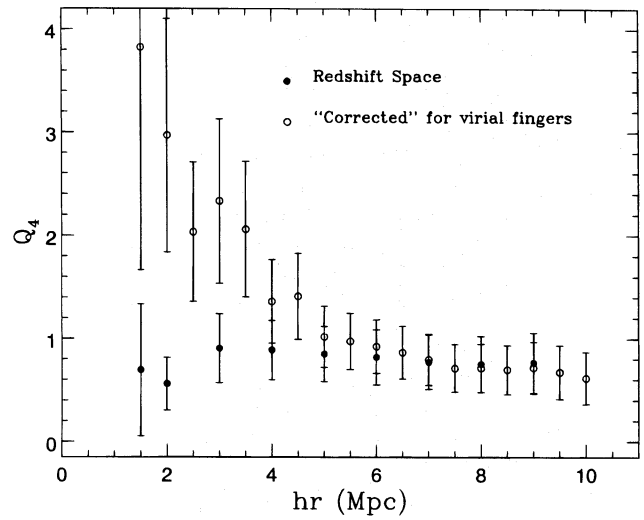

FIG. 2.—Same as Fig. 1, but for the linear combination $Q_4 \equiv Q_{4a}/3 + Q_{4b}$ of the coefficients of the hierarchical four-point function.

fit by a Gaussian, with a typical dispersion of 700 km s^{-1} (see, e.g., Collins et al. 1995). An attempt to bring galaxies back to their most probable real spatial positions can be made by assuming that in real space the cluster radial profile can still be described sufficiently well by a Gaussian, but with a smaller dispersion $\bar{\sigma}$, related to the typical cluster size. This was done for PPS data, where $\bar{\sigma} = 100$ km s^{-1} was adopted. This value was physically motivated by the observed typical projected total radius of $R \geq 1$ Abell clusters in PPS, ranging between 1 and 2 h^{-1} Mpc, i.e., (1–2)$\bar{\sigma}$. Also, with this value of $\bar{\sigma}$, the correct small-scale slope of the two-point correlation function was recovered. According to this technique, galaxies that belong to each finger are marked empirically, and their line-of-sight velocity v_i is corrected following the formula

$$v_i^{\rm corr} = \langle v_{\rm cl} \rangle + (v_i - \langle v_{\rm cl} \rangle)(\bar{\sigma}/\sigma_{\rm cl}) , \quad (1)$$

where $v_{\rm cl}$ is the cluster mean radial velocity. Equation (1) implies the conservation of the total number of galaxies in the cluster when shrinking the cluster to its new, Gaussian shape. Let us remind the reader that this simple procedure allows one to recover the expected real-space $\xi(r)$ and that our aim is to test how higher moments at small separation are affected by it. This test will be performed through the analysis of N-body simulations.

Real and simulated samples are analyzed using the neighbor-moment approach. Neighbor moments can be related to clustering models using suitable relations. A detailed treatment of this point, as well as a comparison between the use of cell and neighbor moments, can be found in BBGKP. The analytical relations used here are given in BIGGH (see also Peebles 1980 and references therein). The measures made on the samples amount to counting the numbers $N_k(r)$ of galaxies in spheres of radius r centered around the kth galaxy. Such numbers are compared with the numbers $n_k(r)$ of points of random samples occupying the same volume of the VLS with the same average density of objects. From these numbers, the quantities $C_{nm}(r) = \langle [N(r)]^n \rangle / \langle [n(r)]^m \rangle$ are estimated. From $C_{nm}(r)$, we work out the parameters of the so-called hierarchical clustering model (HM).

Besides taking $\xi(r) = (r_0/r)^\gamma$, in HM the three- and four-point connected functions read

$$\xi^{(3)}_{123} = Q(\xi_{12}\xi_{13} + \xi_{21}\xi_{23} + \xi_{32}\xi_{31}) , \quad (2)$$

$$\xi^{(4)}_{1234} = Q_{4a}(\xi_{12}\xi_{13}\xi_{14} + \text{symmetric terms}) + Q_{4b}(\xi_{12}\xi_{23}\xi_{34} + \text{symmetric terms}) . \quad (3)$$

The large-scale distribution fits HM if the *hierarchical coefficients* Q, worked out from the C_{nm} for different r, are compatible with a single value.

Our approach to the estimation of errors is carefully described in BIGGH and essentially amounts to a modified bootstrap procedure, which is repeated a large number of times ($\sim$20; bootstrap techniques and their statistical significance are widely discussed in the literature—see, e.g., Ling, Frenk, & Barrow 1986; Efron & Tibshirani 1991). Here we made sure that the error distribution is consistent with a Gaussian one, and the standard deviations we quote are then related to the width of this Gaussian distribution.

We estimated $\xi(r)$ for the redshift-space VLS by applying the standard estimator described in BIGGH, obtaining $r_0 = 8 \pm 1.2\ h^{-1}$ Mpc and $\gamma = 1.24 \pm 0.11$ (3 σ bootstrap errors; note that in redshift space, scales are often indicated

by s instead of r, but we did not adopt this convention since quantities for real and redshift space are shown together in the figures). In Figures 1 and 2 the behaviors of Q and $Q_4 \equiv Q_{4a}/3 + Q_{4b}$ as a function of r are shown, calculated using the same algorithm as BIGGH, whose results are also plotted. Here again error bars correspond to 3 σ (but remember that points for different r are not statistically independent). Figures 1 and 2 show that the redshift-space VLS is fully consistent with HM, quite at variance from the reconstructed-space VLS analyzed in BIGGH: operating in redshift space, no deviation from the HM distribution is left. This is one of the main results of this work.

The fact that the scale dependence of Q found in BIGGH was induced by cluster compression is not enough to conclude that such a dependence is a spurious effect. It is quite possible that cluster compression allows one to recover actual features of the real-space distribution, though it might also lead to overcorrection of data. A deeper analysis of this reconstruction technique can be performed by considering the results of N-body simulations, as we do in the next section.

3. SIMULATION RESULTS IN REAL, REDSHIFT, AND RECONSTRUCTED SPACE

In this section we shall use the particle-mesh simulations performed by Klypin et al. (1995), which evolved 50 h^{-1} Mpc cubes, with a formal resolution of 97.7 h^{-1} kpc, thanks to a 512^3 set of grid points. Four different simulations are considered: two realizations of the cold plus hot dark matter model ($CDHM_1$, $CDHM_2$), and a cold dark matter model with bias factors $b = 1.5$ (CDM1.5) and 1 (CDM1). Further details can be found in BBGKP.

Our goal is a comparison with the PPS volume-limited sample of bright ($M \leq -19 + 5 \log h$) galaxies. Simulation outputs will therefore be used to locate *galaxies* and to attribute to them suitable peculiar velocities. The resultant real-space distribution can then be studied directly or used to work out a *redshift-space* distribution, taking peculiar velocities into account. A further step will then amount to applying the compression procedure used to eliminate virial fingers to such artificial redshift space, as done for the rich clusters of PPS. In this way we produce artificial data similar to the *reconstructed* real space of PPS, but—differently from real data—we shall also control the original real-space distribution.

We locate galaxies in the high-density peaks of the simulation box (peaks are local density maxima on the 512^3 grid; see also Klypin et al. 1993). We assign a mass M_k to the kth peak by averaging over a 27 cell cube, whose side is $s = 293\ h^{-1}$ kpc, and the number of galaxies associated to it is assumed to be *roughly* (see below) proportional to its mass M_k. Only peaks above some suitable mass threshold $m_{\rm th}$ are considered. We fix $m_{\rm th}$ by requiring that two conditions are implemented: (1) the typical mass corresponding to one galaxy is $\sim m_{\rm th}$; (2) the number density of galaxies, obtained with such threshold in the simulation box, coincides with the number density n of galaxies in our VLS.

In more detail, let l be the side of the box. $N^{(g)} = nl^3$ galaxies will be set in $N^{(p)}$ ($\leq N^{(g)}$) peaks with mass $M_k \geq m_{\rm th}$ such that $\sum_{k=1}^{N(p)} \text{int}\,(M_k/m_{\rm th}) = N^{(g)}$. The $v_k = \text{int}\,(M_k/m_{\rm th})$ galaxies of the kth peak should be given a mass $m_k = M_k/v_k$; clearly, $m_{\rm th} \leq m_k < 2m_{\rm th}$, but many peaks yield $v_k \gg 1$, and therefore most m_k are just slightly above $m_{\rm th}$. Such a mass distribution is not related to the actual mass function and is therefore replaced by an equal mass $\bar{m}$ (slightly above $m_{\rm th}$) for all galaxies. (We have also implemented an algorithm able to distribute the mass according to a Schechter law; details are given in Ghigna et al. 1994. The use of such algorithm here would complicate the analysis and does not modify the conclusions obtained in this work through the above, simpler model.)

In order to work out the redshift-space distribution of these *galaxies*, the essential ingredient is individual galaxy velocities. Simulation outputs provide coordinates and velocities for each peak, but this is not enough. Virial equilibrium in the kth peak prescribes that the v_k galaxies it contains have an rms velocity $\bar{v}_k \simeq (4\pi/3)^{1/6} v_k^{1/2} (G\bar{m}/s)^{1/2} = 86\{v_k h[\bar{m}/(10^{10} M_\odot)]\}^{1/2}$ km s^{-1}. With $v_k \sim 10$, the assumption of virial-equilibrium velocities can displace individual galaxies by some megaparsecs from the position of the peak in the redshift space. In Figure 3, we plot the overall distribution of velocities along a given line of sight, relative to peaks, obtained by attributing Maxwellian velocities to galaxies (mean square velocity $\bar{v}_k$ within the kth peak) in random directions. This shows how relevant expected velocities inside peaks are to inducing distortions in redshift space. (Note the remarkable difference between the CHDM and CDM models.)

The redshift-space galaxy distribution is obtained by taking virial velocities into account. This is a good approximation for large v_k, but for small peaks, yielding just a few galaxies, it is clearly a simplified choice. Nonetheless, it allows us to keep the number of free parameters as small as possible; we checked that this prescription provides a two-point function in artificial samples consistent with the one measured for PPS. We constructed several VLSs with shape and volume equal to the $M \leq -19$ PPS subsample. In doing this, a problem arises from the upper limit to the depth obtainable in our 50 h^{-1} Mpc box, which is 86.6 h^{-1} Mpc along its diagonal. The depth of the observational VLS (79 h^{-1} Mpc) lies within the box only within a small solid angle around its diagonal. Outside of this angle, replicas of the points of the simulation box are to be constructed by exploiting the periodic boundary conditions. However, a few points are included in an artificial VLS together with their replicas. This multiple use occurs only for $\sim$15% of them. Moreover, at points used more than once, the line of sight is always differently directed. Of course, a larger simulation box would be welcome, but note that here we are concerned with the behavior of clustering and velocities over scales smaller than $r_0 \sim 8\ h^{-1}$ Mpc, while replicated volumes are always separated by distances almost 10 times greater, and the greater weight given to those few points used multiply allows us to reproduce the impact of the VLS geometry in a fully safe way. Here we never seek correlations among points that are mutual replicas, while the structure of the borders could affect the behavior on relatively small scales.

However, any residual risk of overweighting the features of some portion of the simulation volume is overcome by testing the impact of changing the origin, i.e., the point where we place the observer, and/or the direction of the axis of the conoid with respect to the diagonal of the simulation box. No significant dependence on these changes was detected.

In order to apply a compression procedure analogous to that applied to PPS to the artificial samples, we have to identify galaxy concentrations analogous to Abell groups.

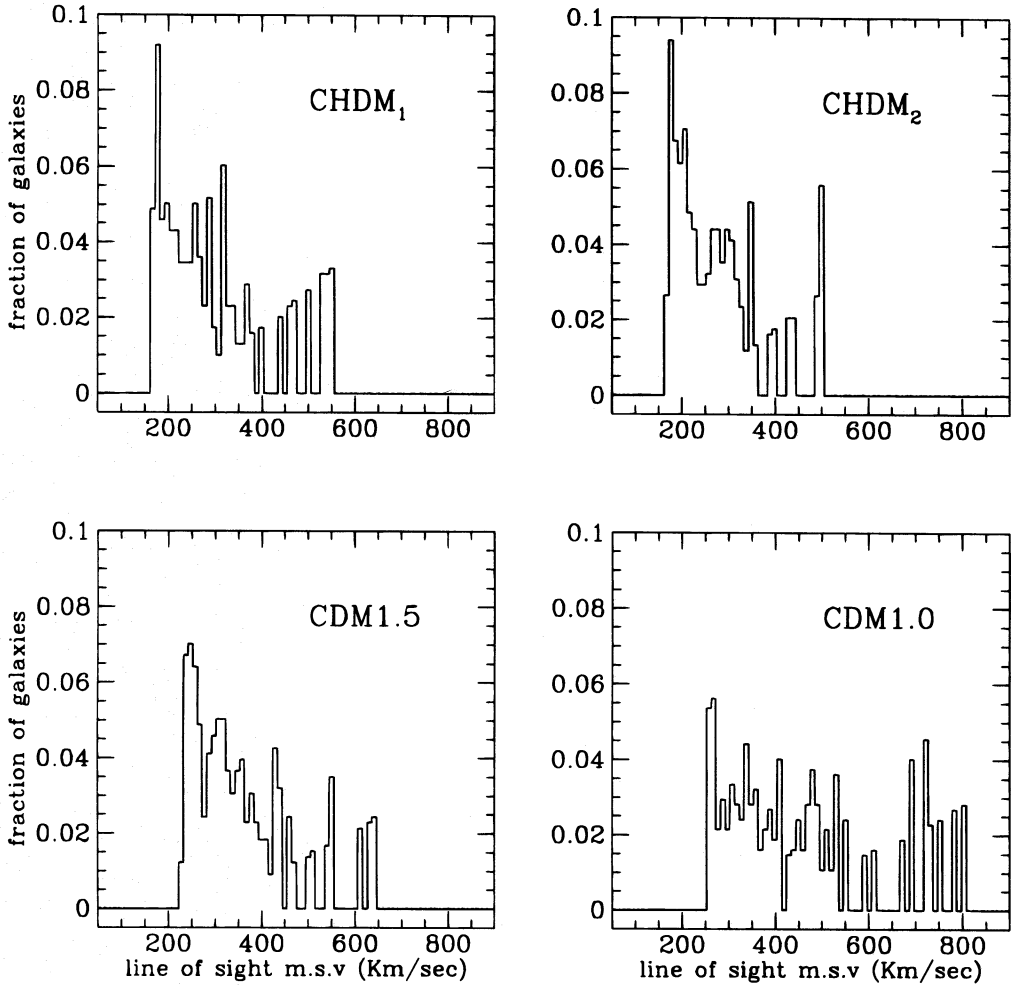

FIG. 3.—Distribution of the line-of-sight mean square velocities (m.s.v.) of galaxies, relative to peaks, estimated through the virial theorem. Only those galaxies that have at least one companion inside the same peak are considered (solely in this case, a peculiar velocity relative to the peak rest frame is assigned to the galaxies). The histograms show the fraction of galaxies in bins of 10 km s^{-1} for the two runs of the cold plus hot dark matter model ($CHDM_1$, $CHDM_2$) and for cold dark matter with bias $b = 1.5$ (CDM1.5) and without bias (CDM1).

In the real sky, such groups are identified through angular data limited in apparent magnitude. In principle, it would be possible to proceed on quite similar grounds for artificial data as well. Rather than going through such a complicated procedure, we preferred to work directly on three-dimensional spatial data. After a smoothing of the density field by a Gaussian window function with smoothing length $r_a = 1.5\ h^{-1}$ Mpc (roughly an Abell radius), we selected the four highest peaks of the smoothed field contained in the sample boundaries (four is the number of Abell groups used

TABLE 1

RESULTS OF FIRST CHDM MODEL RUN

r (h^{-1} Mpc)	Real Space ($Q_{rl.s}$)	Redshift Space ($Q_{rd.s}$)	Reconstructed Real Space ($Q_{r.rl.s}$)	$\frac{\lvert Q_{rl.s} - Q_{r.rl.s}\rvert}{\sigma_{rl.s}}$
0.5	0.7114 ± 0.0140	0.5350 ± 0.0832	1.0286 ± 0.0401	5.9
1.5	0.7418 ± 0.0194	0.6192 ± 0.0149	0.9780 ± 0.0264	5.2
2.4	0.6308 ± 0.0148	0.5964 ± 0.0139	0.8099 ± 0.0119	6.7
3.4	0.5923 ± 0.0100	0.5931 ± 0.0092	0.6696 ± 0.0088	4.1
4.4	0.5918 ± 0.0108	0.6031 ± 0.0087	0.6155 ± 0.0071	1.3
5.4	0.5775 ± 0.0087	0.6023 ± 0.0096	0.5978 ± 0.0094	1.1
6.3	0.5681 ± 0.0088	0.5865 ± 0.0065	0.5701 ± 0.0083	0.1
7.3	0.5703 ± 0.0090	0.5675 ± 0.0062	0.5465 ± 0.0071	1.5
8.3	0.5508 ± 0.0086	0.5604 ± 0.0074	0.5407 ± 0.0075	0.6
9.3	0.5339 ± 0.0081	0.5570 ± 0.0086	0.5269 ± 0.0071	0.5

NOTES.—Values of the hierarchical coefficient Q at varying scale r for the first run of the cold plus hot dark matter model ($CHDM_1$). Each value is accompanied by its standard deviation (1 σ bootstrap error). Data are shown for the galaxy distribution in real space, in redshift space, and in reconstructed real space, where a compression of rich galaxy groups, aimed at eliminating virial fingers, was performed. The last column lists the number of standard deviations that separates the real-space values and the corresponding values in reconstructed space.

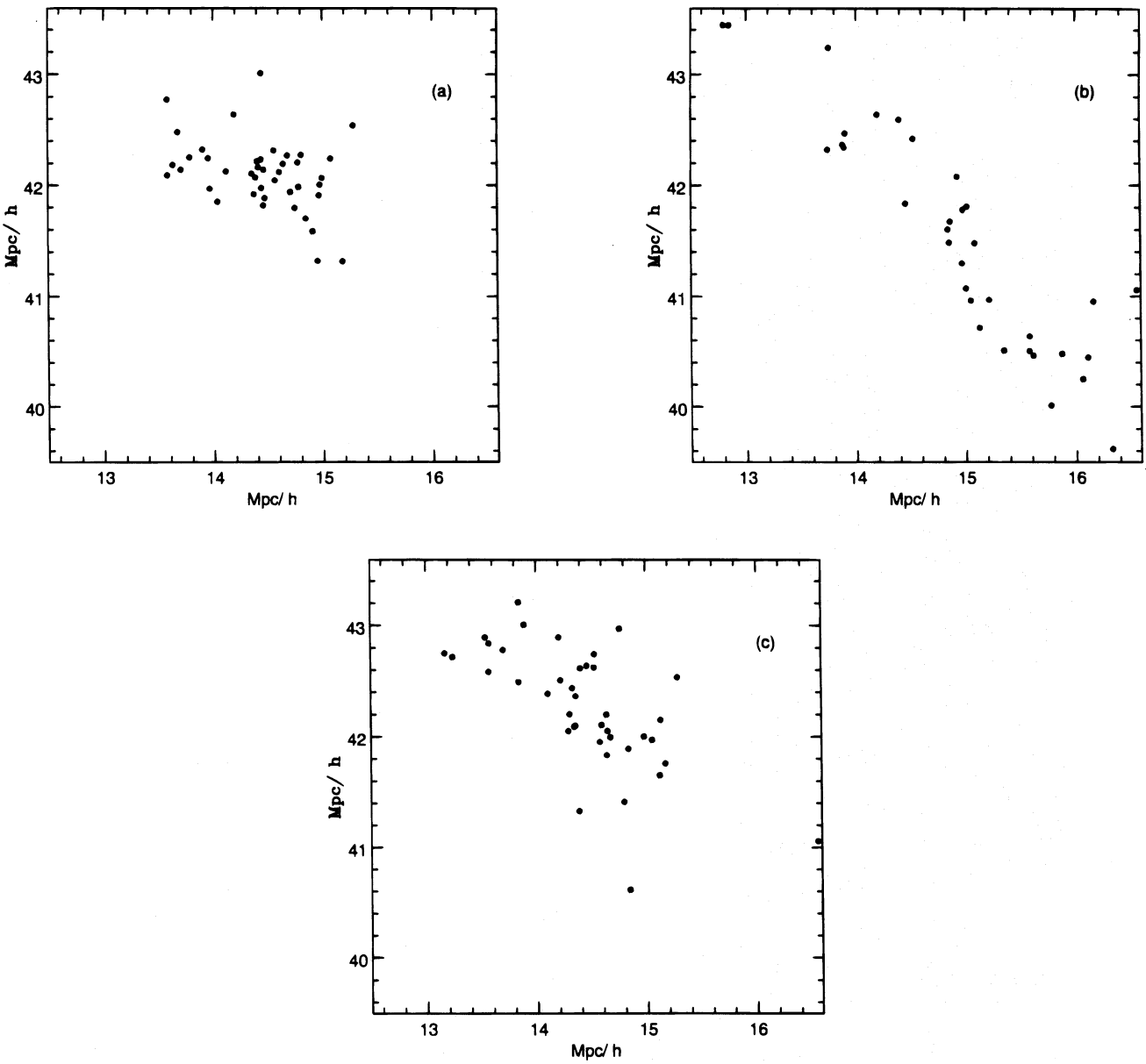

FIG. 4.—Effect of the virial-finger compression technique for a rich cluster of the CHDM$_2$ simulation. A slice of thickness 3 h^{-1} Mpc containing the cluster is shown in (*a*) real space, (*b*) redshift space, and (*c*) reconstructed real space (where the finger compression is performed). The observer has coordinates (25, 25) and is placed in the plane of the slice, so in practice the line of sight is parallel to the descending diagonal of the square (top left to bottom right).

for compression in PPS). The galaxies within a distance r_a from the peak were then treated as cluster members, and the compression procedure was applied to their distribution in the redshift space. As an example, in Figure 4 we show what happens to the galaxies of a rich cluster of the CHDM$_2$ simulation.

In Figures 5–8, we plot the hierarchical coefficients Q and Q_4 of the three- and four-point functions as a function of

TABLE 2

RESULTS OF SECOND CHDM MODEL RUN (CHDM$_2$)

r (h^{-1} Mpc)	Real Space ($Q_{\rm rl.s}$)	Redshift Space ($Q_{\rm rd.s}$)	Reconstructed Real Space ($Q_{\rm r.rl.s}$)	$\frac{\lvert Q_{\rm rl.s} - Q_{\rm r.rl.s}\rvert}{\sigma_{\rm rl.s}}$
0.5	0.8836 ± 0.0251	0.6629 ± 0.0583	1.2430 ± 0.0529	4.6
1.5	0.8100 ± 0.0122	0.6889 ± 0.0210	1.0835 ± 0.0287	6.7
2.4	0.7359 ± 0.0106	0.6122 ± 0.0150	0.9165 ± 0.0210	5.7
3.4	0.6576 ± 0.0102	0.5833 ± 0.0141	0.7429 ± 0.0129	3.7
4.4	0.6081 ± 0.0070	0.5545 ± 0.0102	0.6545 ± 0.0107	2.6
5.4	0.5662 ± 0.0046	0.5418 ± 0.0088	0.6016 ± 0.0076	2.9
6.3	0.5345 ± 0.0032	0.5320 ± 0.0084	0.5693 ± 0.0054	4.1
7.3	0.5046 ± 0.0033	0.5149 ± 0.0075	0.5279 ± 0.0044	3.0
8.3	0.4859 ± 0.0029	0.5039 ± 0.0062	0.5030 ± 0.0037	2.6
9.3	0.4719 ± 0.0024	0.4893 ± 0.0057	0.4890 ± 0.0024	3.6

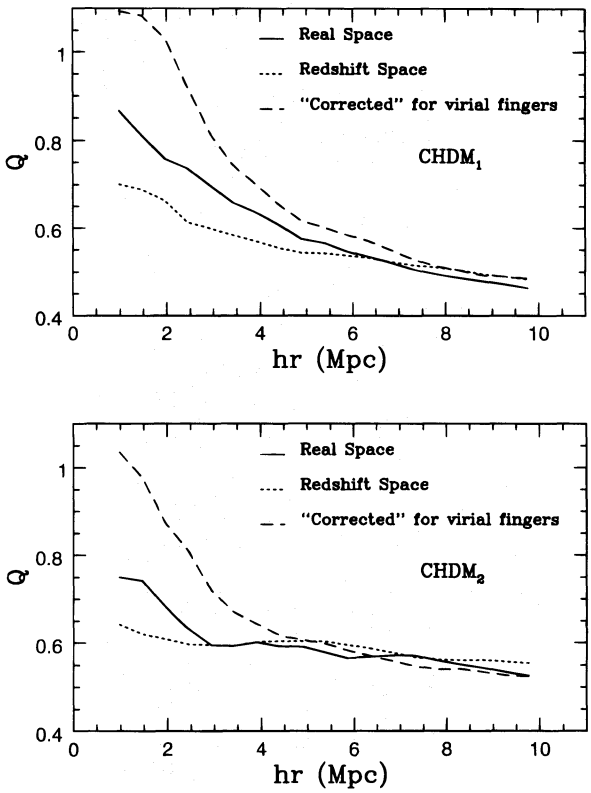

FIG. 5.—Hierarchical coefficient Q (three-point function) at varying scale for the VLSs built up from the simulation outputs for real, redshift, and reconstructed space, for $CHDM_1$ (*top*) and $CHDM_2$ (*bottom*). To avoid confusion, error bars are not shown; 1 σ errors are listed in Tables 1 and 2.

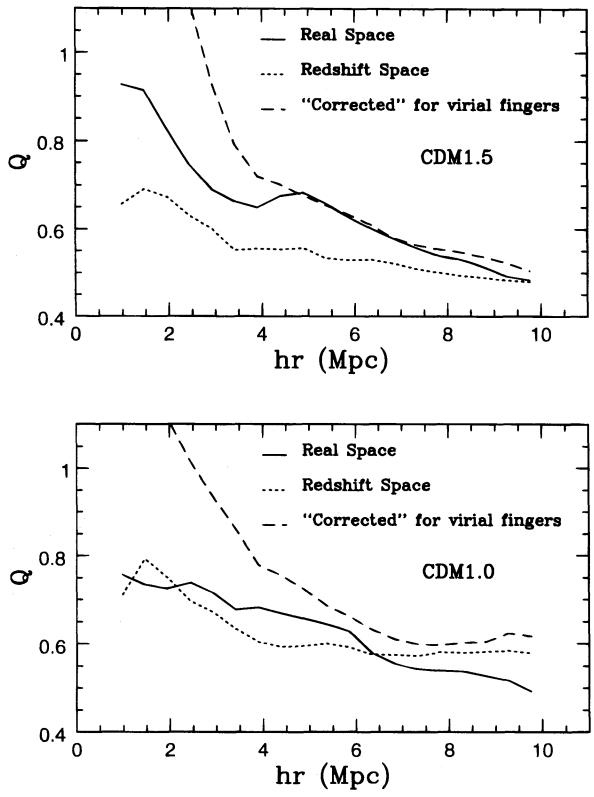

FIG. 6.—Same as Fig. 5, but for CDM1.5 (*top*) and CDM1 (*bottom*); Table 3 lists 1 σ errors.

scale, comparing real space, redshift space, and reconstructed space, for the four simulations considered. We refrained from plotting error bars, to avoid confusion. In Tables 1–3, Q-values for $CHDM_1$, $CHDM_2$, and CDM1 are reported and supplied with bootstrap errors (1 σ). In the last column of each table the number of standard deviations between real-space and reconstructed-space results are shown. Error bars for other cases are essentially similar.

4. DISCUSSION

That the passage from real to redshift space could damp deviations from HM has been claimed elsewhere, by authors analyzing simulations to verify whether they support HM. For example, Bouchet & Hernquist (1992) and Lahav et al. (1992) found deviations from HM at the scale corresponding to the transition from the linear to the nonlinear regime (~ 3–$5\ h^{-1}$ Mpc). They considered this to be at variance with redshift-space observational data and ascribed the discrepancy to redshift-space distortions, suggesting that HM parameters appear more constant in redshift space than in real space. Colombi, Bouchet, & Schaeffer (1993) interpreted discrepancies from HM as due just to lack of statistics. Fry & Gaztañaga (1994) also attempted to compare real- and redshift-space behaviors for various models, within the count-in-cells approach. They were unable to detect deviations from HM. In two recent papers, Matsubara & Suto (1994) and Suto & Matsubara (1994) examined the effects of passing to redshift space on the basis of CDM N-body simulations. They also found that any signature of nonhierarchical behavior in real space is erased by the passage to redshift space.

In most of these papers, deviations from HM were found in the behavior of dark matter particles and through the

TABLE 3

RESULTS OF UNBIASED CDM MODEL RUN (CDM1)

r (h^{-1} Mpc)	Real Space ($Q_{\rm rl.s}$)	Redshift Space ($Q_{\rm rd.s}$)	Reconstructed Real Space ($Q_{\rm r.rl.s}$)	$\frac{\lvert Q_{\rm rl.s} - Q_{\rm r.rl.s}\rvert}{\sigma_{\rm rl.s}}$
0.5	0.7031 ± 0.0134	0.7334 ± 0.1825	1.6286 ± 0.0608	12.5
1.5	0.7337 ± 0.0110	0.7920 ± 0.0422	1.2181 ± 0.0260	13.1
2.4	0.7384 ± 0.0078	0.6961 ± 0.0245	1.0148 ± 0.0137	12.8
3.4	0.6769 ± 0.0049	0.6338 ± 0.0227	0.8613 ± 0.0105	11.9
4.4	0.6693 ± 0.0048	0.5932 ± 0.0145	0.7549 ± 0.0150	4.3
5.4	0.6443 ± 0.0048	0.6004 ± 0.0139	0.6859 ± 0.0117	2.5
6.3	0.5789 ± 0.0037	0.5752 ± 0.0133	0.6312 ± 0.0118	3.4
7.3	0.5423 ± 0.0052	0.5721 ± 0.0094	0.5984 ± 0.0104	3.6
8.3	0.5380 ± 0.0071	0.5798 ± 0.0077	0.6020 ± 0.0109	3.6
9.3	0.5170 ± 0.0087	0.5845 ± 0.0058	0.6235 ± 0.0119	5.2

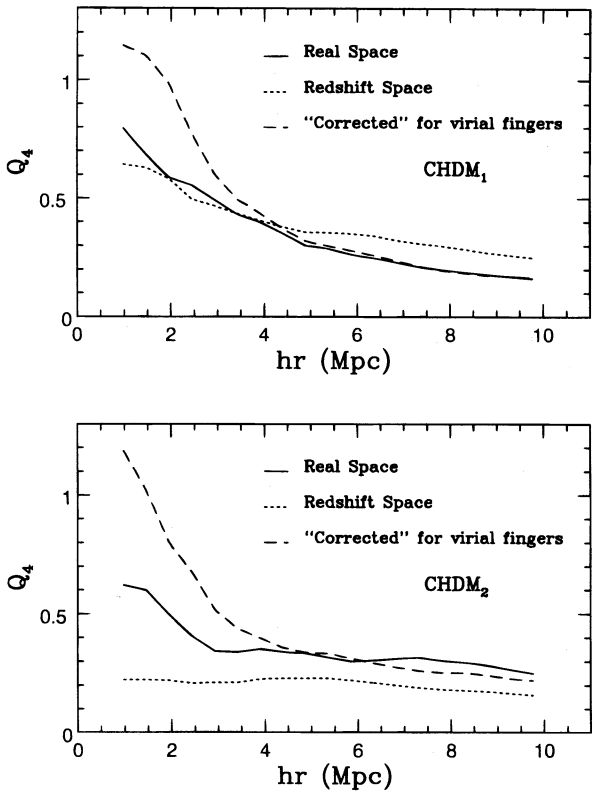

FIG. 7.—Same as Fig. 5, but for the hierarchical coefficient Q_4 (four-point function).

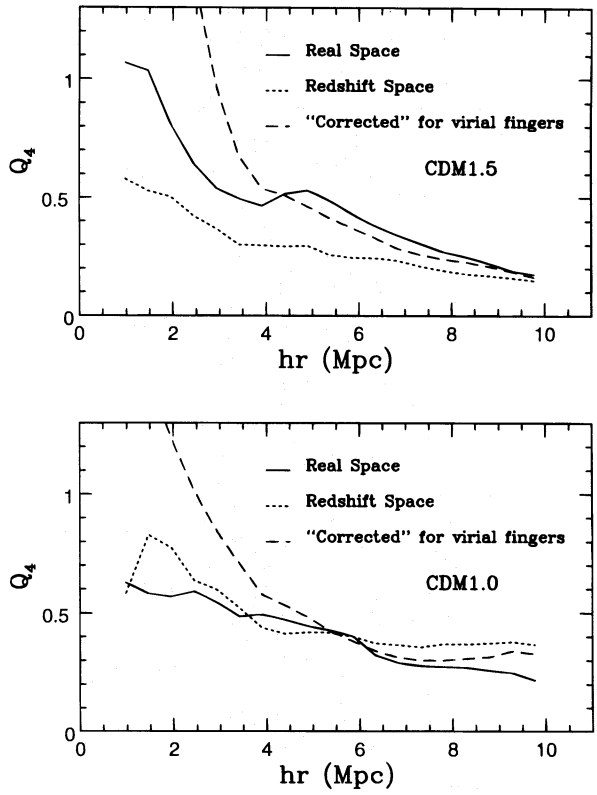

FIG. 8.—Same as Fig. 7, but for CDM1.5 (*top*) and CDM1 (*bottom*)

study of the count-in-cells moments. Such deviations are stronger than those shown here. Still using count-in-cells, in BBGKP it was shown that, although the distribution of dark matter particles exhibits marked deviations from HM, the distribution of galaxies, located in peaks of the simulations, is not affected by substantial deviations from HM, both in real space and in redshift space. BBGKP also showed that the HM violation of dark matter particles could be a natural consequence of scarce sampling. It is, however, confirmed that such violation is depressed by the passage to redshift space.

We can also outline that, in the analysis of observational data, the scale dependence of clustering coefficients found here is quite similar to that found by Gaztañaga (1994) by examining the Automatic Plate Measuring angular data (but see Szapudi et al. 1995).

The shape of the dependence of Q on r found in the analysis of real-space distributions for *biased* models can be related to a clustering model different from HM. If one assumes that

$$\langle \delta N_1 \cdots \delta N_k \rangle = \delta V_1 \cdots \delta V_k n_V^k \prod_{i<j=1}^{k} (1 + \xi_{ij}) \qquad (4)$$

(i.e., the Kirkwood superposition expression, hereafter KW), the connected three-point function reads

$$\xi^{(3)}_{123} = Q(\xi_{12}\xi_{13} + \xi_{21}\xi_{23} + \xi_{32}\xi_{31}) + Q'\xi_{12}\xi_{23}\xi_{31} , \qquad (5)$$

with $Q = Q' = 1$. In a similar fashion, the four-point connected function contains terms up to the sixth degree in ξ, with fixed coefficients. In BIGGH it was shown that a better fit to the data is obtained with a KW-like expression, but with $Q = Q' \neq 1$ (similar results hold for the four-point function). On the contrary, fitting the data by the HM expressions (eqs. [2], [3]) yields coefficients Q and Q_4 that depend on r, with an increasing trend toward small scales. In the following we will refer to this case as "KW-like" behavior of the coefficients.

KW-like expressions, as in equations (4) and (5), are obtained within the theory of biased galaxy formation (Jensen & Szalay 1986; Matarrese, Lucchin, & Bonometto 1986; Szalay 1988; Borgani & Bonometto 1990), assuming that no displacements of galaxies took place from the sites where they formed. However, displacements occur during the evolution of structures via gravitational instability; they can be inferred from galaxy peculiar velocities. Zurek et al. (1993) have corrected the value originally found by Davis & Peebles (1983) for the rms one-dimensional pairwise velocity dispersion at 1 h^{-1} Mpc. The values they found are in the range 400–500 km s^{-1}. Although the size and richness of the samples available are not enough to accurately deduce the shape of the distribution about the average velocity, such distribution still leaves a fair amount of galaxies in the 100–200 h^{-1} km s^{-1} range. In a Hubble time (H^{-1}), these velocities correspond to displacements of $\sim$1–2 h^{-1} Mpc. Accordingly, it can be expected that galaxy proper motions cancel KW-like features below 1–2 h^{-1} Mpc and significantly attenuate them up to 4–5 h^{-1} Mpc. Slightly above the latter limit we enter the linear regime, where higher power terms in expressions like equation (5) become less and less important and no distinction can be made between KW and HM (the term in eq. [5] with coefficient Q' becomes negligible).

Deviations of Q and Q_4 from HM predictions, in the form of a residual KW-like behavior related to biased galaxy formation, can therefore be expected to be still visible *in the real space* in the range 2–5 h^{-1} Mpc. The passage to redshift

space should erase such residual features, doubling the effect of peculiar velocities (see § 1). The behavior of the *COBE*-compatible CDM simulation (CDM1, with $b = 1$, i.e., *unbiased*), where the KW-like regime is at least very attenuated, is a possible countercheck. Unbiased CDM is known to lead to high peculiar velocities, likely to exceed the observational range; furthermore, the choice of $b = 1$ leaves little room for arguments connected with biased theories of galaxy formation. So, CDM1 should show no difference between real- and redshift-space behaviors of hierarchical coefficients. Indeed, taking into account bootstrap errors, the real-space and redshift-space curves for CDM1 are nearly compatible with constants.

In reconstructed space, however, *all* models show a KW-like behavior. This prompts the main conclusion of this work: although the KW-like behavior detected in reconstructed space for PPS data is consistent with a similar behavior of simulated data in real space, we cannot conclude that this nonhierarchicality is an actual feature of PPS data. In fact, it is apparent that the compression technique itself creates a KW-like behavior and can do so in the absence of such behavior in the real space. Therefore, it seems that the subject of deviations from hierarchicality can hardly be debated by examining redshift-survey data. If deviations exist, they tend to be hidden by redshift-space distortions, and reconstruction techniques for the real-space distribution could easily add spurious effects, as in the simple model considered here.

A remark that follows from this result is that Abell clusters are dominant in the detection of three- and four-point function signals. Let δP_0 be the probability of finding a galaxy in a given volume δV_0 and n_V be the average number of galaxies per unit volume. Quite independently of detailed theoretical models, the presence of a positive three-point connected function tells us that if two galaxies G_1 and G_2 are at distances r_1 and r_2 from δV_0, then δP_0 does not only exceed $n_V \delta V_0$, but the excess is greater than the sum of the enhancements due to the presence of G_1 and G_2 separately. The critical quantity is therefore the difference between the overall excess and the two separate enhancements. In HM, its scale dependence is roughly proportional to ξ^2. The violations we find of HM tend to indicate that the difference increases even more steeply at scales below 3–4 h^{-1} Mpc. Similar statements can be made for the four-point function. In the passage from redshift space to reconstructed space, such violations appear to be caused by galaxies in Abell clusters. This seems to indicate that, on average, the *compressed* clusters have volumes that are relatively too small, and therefore the number density inside them has too steep a decline. In general, Abell clusters should not be given an isotropic shape. They ought to be kept elongated, although their actual elongation is certainly not always toward the observer, as in redshift space. Since any simplification adopted in the compression procedure seems to have a strong impact on high-order correlation functions, we feel that even more realistic reconstruction techniques than the one used here would always be unsafe in recovering the real-space distribution of galaxies.

Thanks are due to Stefano Borgani and Angela Iovino for discussions. Angela Iovino also kindly allowed us to make use of an algorithm she had collaborated to build for a previous analysis. Thanks are also due to an anonymous referee, who forced us to inspect the reconstructed space for artificial data, from which we gained a significantly improved understanding of the overall matter.

REFERENCES

Bonometto, S. A., Borgani, S., Ghigna, S., Klypin, A., & Primack, J. 1994, MNRAS, 273, 101 (BBGKP)
Bonometto, S. A., Iovino, A., Guzzo, L., Giovanelli, R., & Haynes, M. 1993, ApJ, 419, 451 (BIGGH)
Borgani, S., & Bonometto, S. A. 1990, ApJ, 338, 398
Bouchet, F. R., & Hernquist, L. 1992, ApJ, 400, 25
Burstein, D., & Heiles, C. 1978, ApJ, 225, 40
Cole, S., Fisher, K. B., & Weinberg, D. H. 1994, MNRAS, 267, 785
———. 1995, MNRAS, 275, 515
Collins, C. A., Guzzo, L., Nichol, R. C., & Lumsden, S. L. 1995, MNRAS, 276, 689
Colombi, S., Bouchet, F. R., & Schaeffer, R. 1993, A&A, 263, 1
Davis, M., & Peebles, P. J. E. 1983, ApJ, 267, 465
Efron, B., & Tibshirani, R. 1991, Science, 253, 390
Fisher, K. B., Davis, M., Strauss, M. A., Yahil, A., & Huchra, J. P. 1994, MNRAS, 266, 50
Fry, J. N., & Gaztañaga, E. 1994, ApJ, 425, 1
Fry, J. N., & Peebles, P. J. E. 1978, ApJ, 221, 19
Gaztañaga, E. 1994, MNRAS, 268, 913
Ghigna, S., Borgani, S., Bonometto, S. A., Guzzo, L., Klypin, A., Primack, J. R., Giovanelli, R., & Haynes, M. P. 1994, ApJ, 437, L71
Giovanelli, R., & Haynes, M. P. 1989, AJ, 97, 633
———. 1991, ARA&A, 29, 499
———. 1996, in preparation
Giovanelli, R., Haynes, M. P., & Chincarini, G. 1986, ApJ, 300, 77
Gramann, M., Cen, R., & Bahcall, N. 1993, ApJ, 419, 440
Groth, E. J., & Peebles, P. J. E. 1977, ApJ, 217, 385
Haynes, M. P., Giovanelli, R., Starosta, B. M., & Magri, C. 1988, AJ, 95, 607
Jensen, L. G., & Szalay, A. S. 1986, ApJ, 305, L5
Kaiser, N. 1987, MNRAS, 227, 1
Klypin, A., Holtzman, J., Primack, J., & Regős, E. 1993, ApJ, 416, 1
Klypin, A., Nolthenius, R., & Primack, J. R. 1995, ApJ, submitted (astro-ph/9502062)
Lahav, O., Itoh, M., Inagaki, S., & Suto, Y. 1992, ApJ, 402, 387
Ling, E. N., Frenk, C. S., & Barrow, J. D. 1986, MNRAS, 223, 21P
Matarrese, S., Lucchin, F., & Bonometto, S. A. 1986, ApJ, 310, L21
Matsubara, T., & Suto, Y. 1994, ApJ, 420, 497
Peebles, P. J. E. 1980, The Large-Scale Structure of the Universe (Princeton: Princeton Univ. Press)
Sharp, N. A., Bonometto, S. A., & Lucchin, F. 1984, A&A, 130, 79
Suto, Y., & Matsubara, T. 1994, ApJ, 420, 504
Szalay, A. S. 1988, ApJ, 333, 21
Szapudi, I., Dalton, G., Szalay, A. S., & Efstathiou, G. P. 1995, ApJ, 444, 520
Wegner, G. A., Haynes, M. P., & Giovanelli, R. 1993, AJ, 105, 1251
Yahil, A., Tammann, G. A., & Sandage, A. 1977, ApJ, 217, 903
Zurek, W. H., Warren, M. S., Quinn, P. J., & Salmon, J. K. 1993, in Cosmic Velocity Fields, ed. F. R. Bouchet & M. Lachieze-Rey (Gif-sur-Yvette: Editions Frontières), 465